Doping effects on structural and magnetic evolutions of orthoferrite $SmFe_{(1-x)}Al_xO_3$*

Li Na-Na(李娜娜), Li Hui(李 会), Tang Rui-Lian(唐瑞莲), Han Dan-Dan(韩丹丹), Zhao Yong-Sheng(赵永胜), Gao Wei(高 伟), Zhu Pin-Wen(朱品文)†, and Wang Xin(王 欣)‡

State Key Laboratory of Superhard Materials, Jilin University, Changchun 130012, *China*

(Received 9 August 2013; revised manuscript received 14 November 2013; published online 20 February 2014)

The structural and magnetic properties of $SmFeO_3$ with B site substitution of non-magnetic atom Al are investigated. The x-ray diffraction patterns show that $SmFe_{(1-x)}Al_xO_3$ remains an orthorhombic structure within the whole doping range, and the unit-cell volume decreases monotonically with the increase of doped Al concentration. Besides, the octahedral tilting distortions of FeO_6 are found to be alleviated while the tolerance factor increases. However, the relationship between the lattice parameters and Al concentration is observed to deviate from Vegard's rule, and this may be caused by magnetostriction effects. For the doping content values in a range $0 \leq x \leq 0.6$, the ferromagnetism, antiferromagnetism, and paramagnetism are observed to occur continuously. Moreover, the magnetization and the spin reorientation temperature (T_k) decrease monotonically as Al content value increases. With the doping content values being $x = 0.8$ and 1.0, these compounds only show paramagnetic behavior.

Keywords: magnetic materials, X-ray diffraction, magnetic properties

PACS: 61.05.cp, 61.50.–f, 75.60.–d, 75.30.Et **DOI:** 10.1088/1674-1056/23/4/046105

1. Introduction

The rare-earth (RE) orthoferrite $REFeO_3$ that normally crystallizes into a distorted orthorhombic structure with space group *Pbnm* is a derivative of cubic perovskite.[1] Attributed to the unique physical and chemical properties, these compounds with a perovskite structure are promising for a variety of potential applications such as catalysts, gas separators, cathodes of solid oxide fuel cells, sensor materials, magneto–optic materials, spin valves, etc.[2–11] $SmFeO_3$, as one of RE orthoferrites, has attracted much attention due to its remarkable physical properties like high dielectric constant of 10^4 at room temperature, high T_N temperature ($T_N = 674$ K), and spontaneous magnetization reversal at cryogenic temperatures.[12–14]

In $SmFeO_3$, it has different types of magnetic interactions between Fe^{3+}–Fe^{3+}, Fe^{3+}–Sm^{3+}, and Sm^{3+}–Sm^{3+} consisting of the isotropic, the antisymmetric, and the anisotropic–symmetric superexchange interactions. The anisotropic parts of the magnetic interaction between Fe^{3+} and Sm^{3+} spins with the antisymmetric and the anisotropic–symmetric exchange interactions will determine the spin-reorientation temperature, which can be affected by the substitution of nonmagnetic ions (Al, Ga, etc.). It has been suggested that magnetic vacancies of $REFeO_3$ could induce additional anisotropy, and thus modify properties, not only magnetic but also elastic, thermal, optical, etc., in these compounds. Since the introduction of magnetic vacancies into the Fe sublattice by substitution of nonmagnetic ions makes the system more anisotropic, the dilution effects cannot be neglected even for a small concentration of vacancies and their relevance strongly depends on the nature of the RE ion. For instance, the Morin phase transition temperature increased with the increase of Al doping in $DyFe_xAl_{1-x}O_3$;[15] the reorientation transition temperature decreased while the Tb long-range was inhibited in $TbFe_xAl_{1-x}O_3$;[16] a similar change was also observed in $NdFe_xCo_{1-x}O_3$, in which Co was in a low-spin state.[17] Even in $HoFe_xAl_{1-x}O_3$, a new transition to $\Gamma 1$ magnetic structure was induced by Fe vacancies.[18] In order to further investigate and complement the nonmagnetic doping effects on the structural and magnetic properties in these RE orthoferrites, we systemically study the structural and magnetic properties of $SmFe_xAl_{(1-x)}O_3$. With the increase of Al content, the lattice distortion is alleviated and the deviation from Vegard's rule is observed. The doping effect on the magnetic behavior evolution is discussed. For $x \leq 0.6$, it is found that the reorientation transition temperature decreases with the increasing of Al content, since the substituted Al breaks the symmetry of the local interactions and weakens the inert magnetic interactions; for $x > 0.6$, the strong magnetic interaction is completely destroyed.

2. Experiment

In our experiment, the stoichiometric Sm_2O_3 (99.99% purity), $Al(NO_3)_3{\cdot}9H_2O$ (99.99% purity), $Fe(NO_3)_3{\cdot}9H_2O$ (99.99% purity), and citric acid (AR) were used as raw materials. Firstly, Sm_2O_3 was dissolved in nitric acid and diluted in

*Project supported by the National Natural Science Foundation of China (Grant No. 51172091).

†Corresponding author. E-mail: zhupw@jlu.edu.cn

‡Corresponding author. E-mail: xin_wang@jlu.edu.cn

© 2014 Chinese Physical Society and IOP Publishing Ltd

distilled water, and then $Al(NO_3)_3{\cdot}9H_2O$ and $Fe(NO_3)_3{\cdot}9H_2O$ were dissolved in distilled water and mixed with the Sm nitrates. Citric acid was added as a fuel to the above solution to yield a citrate/nitrate ratio of 1.2. The mixed solution was continuously stirred using a magnetic agitator. Secondly, the as-prepared solution was evaporated by heating at 353 K until a brown sticky gel was formed. Subsequently, the gel was dried at 373 K and calcined at 1273 K in air for 4 h in order to get rid of nitrogen oxides and carbon oxides and obtain a precursor. Finally, the precursor was calcined at 1473 K in air for 4 h.

The phase purity was detected by powder X-ray diffraction (XRD) measurements using Rigaku Rotaflex X-ray diffractometer with Cu-K_α radiation at room temperature. Magnetic measurements were carried out using a physical properties measurement system (PPMS, Quantum Design). The temperature dependence of the magnetization was measured in a magnetic field up to 1 kOe (1 Oe = 79.5775 A/m) in a temperature range of 5 K–400 K. The experiments were performed in the zero-field cooling. The field dependences of the magnetization were measured up to 30 kOe at $T = 10$ K, 300 K respectively.

3. Results and discussion

The crystal structure of $SmFeO_3$ consists of four equivalent Fe^{3+} ions situated in the octahedral centers formed by six nearest-neighbor oxygen atoms as shown in Fig. 1. The degree of freedom for mismatch between the equilibrium (Sm–O) and (Fe–O) bond lengths could be evaluated by the geometric tolerance factor $t = (r_{Sm} - r_O)/\sqrt{2}(r_{Fe} - r_O)$. Commonly the mismatch between Sm–O and Fe–O bond lengths will introduce the internal stresses that can be alleviated by a cooperative rotation of the octahedral and a corresponding position shift of Sm cation. With doping of smaller Al^{3+} ions, the internal stresses are expected to be alleviated with

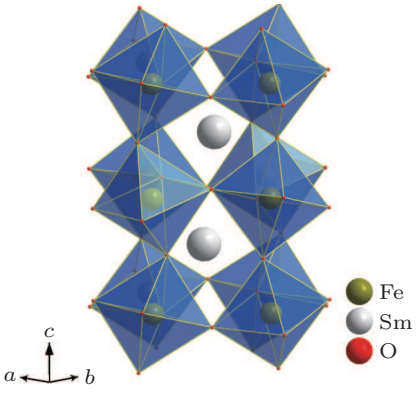


Fig. 1. (color online) Schematic representation of the crystal structure of $SmFeO_3$.

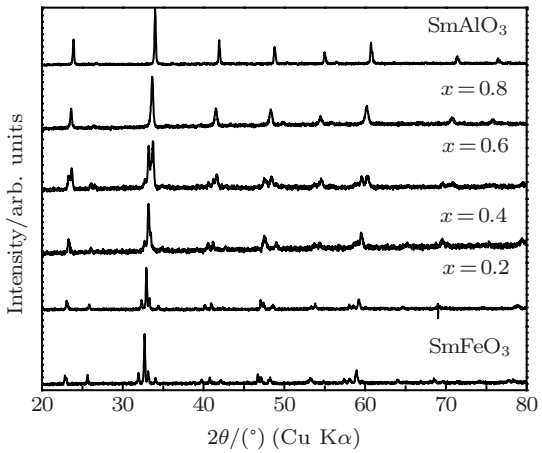


Fig. 2. X-ray diffraction patterns of $SmFe_{(1-x)}Al_xO_3$ ($x = 0.0$, 0.2, 0.4, 0.6, 0.8, 1.0) with incident wavelength $\lambda = 1.5406$ Å at room temperature.

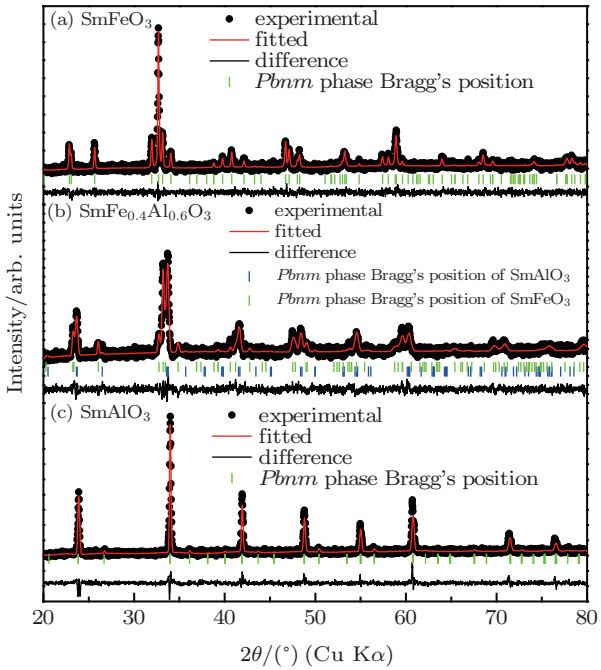


Fig. 3. (color online) Observed, calculated, and difference in X-ray powder patterns of $SmFe_{(1-x)}Al_xO_3$ ($x = 0.0$, 0.6, 1.0): (a) Rietveld refinement of $SmFeO_3$ in orthorhombic (*Pbnm*) phase, (b) Rietveld refinement of $SmFe_{0.4}Al_{0.6}O_3$ both in the phases of $SmFeO_3$ and $SmAlO_3$, and (c) Rietveld refinement of $SmAlO_3$ in orthorhombic (*Pbnm*) phase.

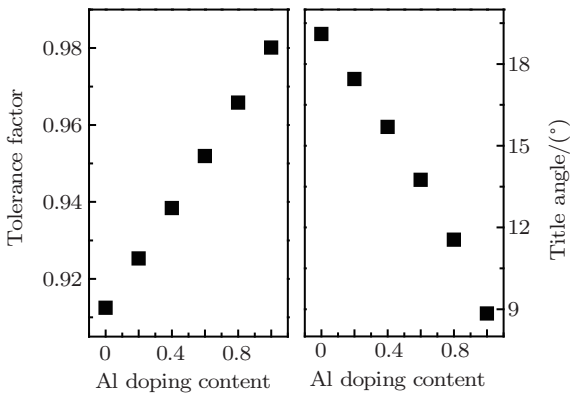


Fig. 4. Tolerance factor and title angle of FeO_6 each as a function of the Al doping content in $SmFeO_6$.

an increase of t value. Figure 2 shows the X-ray diffraction patterns of $SmFe_{(1-x)}Al_xO_3$ (x = 0, 0.2, 0.4, 0.6, 0.8, 1.0). In Fig. 3(a), the diffraction pattern of $SmFeO_3$ was refined in the *Pbnm* phase with the lattice constants of $a = 5.4026(4)$ Å; $b = 5.6001(3)$ Å; $c = 7.7129(7)$ Å by the Rietveld method using the GSAS software.[19] $SmAlO_3$ was also refined in the *Pbnm* phase with the lattice constants of $a = 5.2822(5)$ Å; $b = 5.2733(2)$ Å; $c = 7.4669(4)$ Å as shown in Fig. 3(c). The refined atomic position coordinates and the typical bond lengths and bond angles are given in Table 1. It can be seen that the atomic symmetry of O(1) is different between $SmFeO_3$ and $SmAlO_3$, and the diffraction patterns of $SmFeO_3$ and $SmAlO_3$ are somehow different. It can also be seen that from $SmFeO_3$ to $SmAlO_3$, the bond angle of Fe(Al)–O–Fe(Al) increases and the bond lengths of Fe(Al)–O gradually tends to be equal. It indicates that the octahedral distortion in orthorhombic structure is alleviated with Al doping. During the solid solution, $SmFe_{0.4}Al_{0.6}O_3$ exhibits the clear feature of mixed phases from $SmFeO_3$ and $SmAlO_3$ as can be seen from Fig. 2. Therefore, two phases are simultaneously refined in $SmFe_{0.4}Al_{0.6}O_3$ with merits of $R_{wp} = 5.24\%$ and $R_p = 4.17\%$ as shown in Fig. 3(b). The high quality samples enable us to establish the general relationship between structural and magnetic properties in $SmFeO_3$ upon Al substitution. In order to understand the doping effects on the octahedral tilting distortions in $SmFe_{(1-x)}Al_xO_3$, we use the software SPuDS for our calculations. The optimization procedure is based on the bond-valence method and requires only the composition serving as user inputs.[20] The calculated tolerance factor and the octahedral tilt angle of $SmFe_{(1-x)}Al_xO_3$ are shown in Fig. 4. It is clearly shown that the tolerance factor increases and the octahedral tilt angle of FeO_6 decreases with the increase of Al concentration. It indicates that the lattice distortions are alleviated.

Table 1. Structural parameters of $SmFeO_3$ and $SmAlO_3$ with selected bond angles and bond lengths.

Compounds	$SmFeO_3$	$SmAlO_3$
Crystal system	orthorhombic	orthorhombic
Space group	*Pbnm* (62)	*Pbnm* (62)
a/Å	5.4026(4)	5.2822(5)
b/Å	5.6001(3)	5.2733(2)
c/Å	7.7129(7)	7.4669(4)
Atoms position	Wyckoff (*x y z*)	Wyckoff (*x y z*)
Fe/Al	4*b* (0.5 0 0)	4*b* (0.5 0 0)
Sm	4*c* (0.5134(4) 0.5572(2) 0.25)	4*c* (0.4709(2) 0.4939(1) 0.25)
O(1)	4*c* (0.3958(3) 0.9894(5) 0.25)	8*d* (0.25 0.06911(7) 0.4893(5))
O(2)	8*d* (0.2862(5) 0.6966(4) 0.9613(9))	8*d* (0.0394(4) 0.7255(6) 0.2817(3))
Bond angle/(°): Fe(Al)–O1–Fe(Al)	147.2(2)	157.6(9)
Bond angle/(°): Fe(Al)–O2–Fe(Al)	153.4(1)	157.6(6)
Bond length/Å of Fe(Al)–O1	2.010(6)	2.009(4)
Bond length/Å/ of Fe(Al)–O2	2.076(8), 1.922(7)	1.991(3), 2.052(5)
Residuals[a]/%	R_{wp}: 4.61% R_p: 4.87%	R_{wp}: 7.48% R_p: 5.6%

[a] R_{wp} and R_p as defined in GSAS.[19]

In Fig. 5, the unit cell parameters each as a function of doped Al concentration are given by using a pseudocubic cell. It is evident that the unit-cell volume decreases with the increase of Al concentration, since the ionic radius of Al^{3+} (0.535 Å) is smaller than that of Fe^{3+} (0.645 Å). In general, the orthorhombic (space group *Pbnm*) structure possesses a cooperative rotation about an ideal cubic [110] axis, which is the orthorhombic b axis, and the rotation axis $b/\sqrt{2}$ should be greater than the orthorhombic $a/\sqrt{2}$ and $c/2$ axes. As can be clearly seen in Fig. 5, the lattice constants a_{pc}, b_{pc}, and c_{pc} decrease with the increase of Al content and the difference between their values decreases gradually. Furthermore, the structure is closer to the ideal perovskite structure with $a/\sqrt{2} \approx b/\sqrt{2} \approx c/2$ in $SmAlO_3$. It indicates that the lattice distortions are alleviated due to Al doping. However, by carefully examining the Al concentration dependences of the lattice parameters, deviation from Vegard's rule, especially for $x = 0.6$, can be observed. The result cannot be explained by geometrical origin alone. It seems that the magnetostriction existing in RE orthoferrites can have an influence on this nonlinear behavior. It is supposed that an internal magnetic field induced by weak ferromagnetism will be the source of the above-mentioned magnetostriction in the crystal lattice.[21] As will be discussed below, the magnetic measurements in $SmFe_{(1-x)}Al_xO_3$ exhibit different magnetic behaviors by varying doped Al^{3+} content.

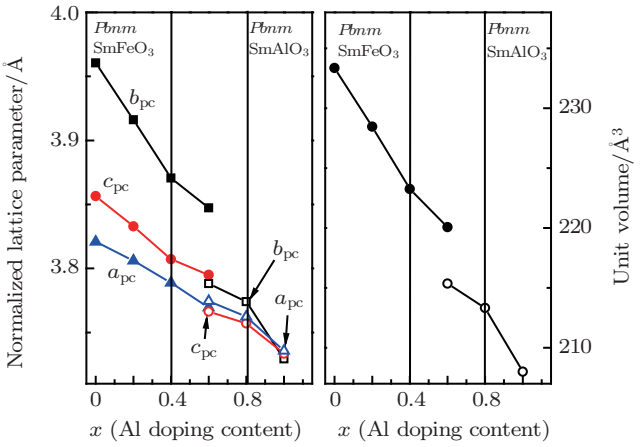


Fig. 5. (color online) Al concentration-dependent lattice parameters and unit cell volume in $SmFe_{(1-x)}Al_xO_3$ ($x = 0.0$, 0.2, 0.4, 0.6, 0.8, 1.0). Solid symbols represent the phase of $SmFeO_3$ and empty symbols for $SmAlO_3$. The cell parameters are described in a pseudocubic cell $a_{pc} = a/\sqrt{2}$, $b_{pc} = b/\sqrt{2}$, and $c_{pc} = c/2$ for the *Pbnm* phase.

The temperature dependences of the magnetization curves of $SmFe_{(1-x)}Al_xO_3$ under an applied field $H = 1$ kOe are shown in Fig. 6. For $SmFeO_3$, the magnetization is 0.335 emu/g at 1 kOe whereas the transition temperature from ferromagnetic to antiferromagnetic is about 230 K. With the increase of the doped Al content, the magnetization and the transition temperature monotonically decrease. For $x = 0.2$ and 0.4, the magnetization values decrease to 0.068 emu/g and 0.063 emu/g with the transition temperature coming down to 180 K and 150 K, respectively. For $x = 0.6$, the magnetization decreases to 0.047 emu/g and the magnetic transition temperature has a large decrease down to 40 K. While in $SmFe_{0.2}Al_{0.8}O_3$ and $SmAlO_3$, they exhibit paramagnetic behaviors as shown in Fig. 7. The inset of Fig. 7 also shows the linear fitting curves complying with the Curie–Weiss law.

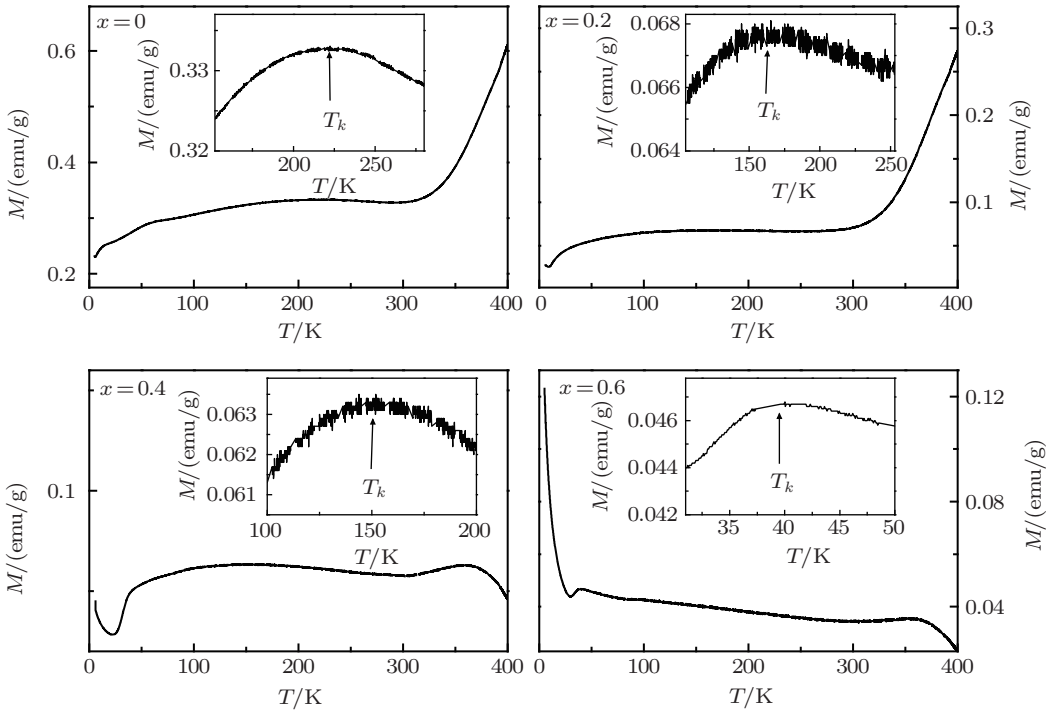


Fig. 6. Temperature-dependent magnetization curves of $SmFe_{(1-x)}Al_xO_3$ ($x = 0.0$, 0.2, 0.4, 0.6) under an applied field $H = 1$ kOe with partial enlarged view.

Upon cooling, the transitions associated with spin reorientations of antiferromagnetically coupled spin moments of RE ions and iron ions have been observed.[22,23] In order to explain the changes of the spin reorientation temperature (T_k) as observed in the M–T curves of $SmFe_{(1-x)}Al_xO_3$, the energies involved in the corresponding interactions among different types of magnetic interactions of Fe^{3+}–Fe^{3+}, Fe^{3+}–Sm^{3+}, and Sm^{3+}–Sm^{3+} must be considered. The competitions of the anisotropic part of the magnetic interaction between Fe^{3+} and Sm^{3+} spins, the antisymmetric and the anisotropic–symmetric exchange interactions will determine the spin-reorientation temperature.[24] Theoretical estimations showed that the non-magnetic substitution not only modified the anisotropy and the RE–Fe interactions in RE orthoferrites, but also (in certain cases) changed the sign of the interactions.[19] And thus RE–Fe coupling could be transformed from ferromagnetic to antiferromagnetic. As a consequence, the lowering of susceptibility would be observed and a compensation point would be generated.[19] In our study, the magnetic dilution of Fe^{3+} sublattice by doping Al^{3+} will lead to a gradual decay of its magnetic bonding system. For $x \leq 0.6$, non-magnetic Al^{3+} ions are randomly distributed in Fe^{3+} sublattice (magnetic

sites) and thus break the symmetry of the local interactions, leading to the decompensation of Fe^{3+}–Fe^{3+} antiferromagnetic interactions in their environment. In addition, it may also weaken the interaction between Fe^{3+}–Sm^{3+} with the nonmagnetic Al doped. Therefore, the magnetization and the transition temperature (T_k) monotonically decrease as Al content increases for $x \leq 0.6$. For $0.8 \leq x \leq 1$, the magnetic vacancies increase drastically, which makes the magnetic interaction between Fe^{3+} and Sm^{3+} very weak. In this case, the magnetic property is mainly determined by magnetic interactions of Sm^{3+}–Sm^{3+}. Moreover, only very weak exchange interactions can take place and the spin reorientation will disappear in Sm^{3+} sublattice. As a result, $SmFe_{(1-x)}Al_xO_3$ ($0.8 \leq x \leq 1$) exhibites paramagnetic behavior.

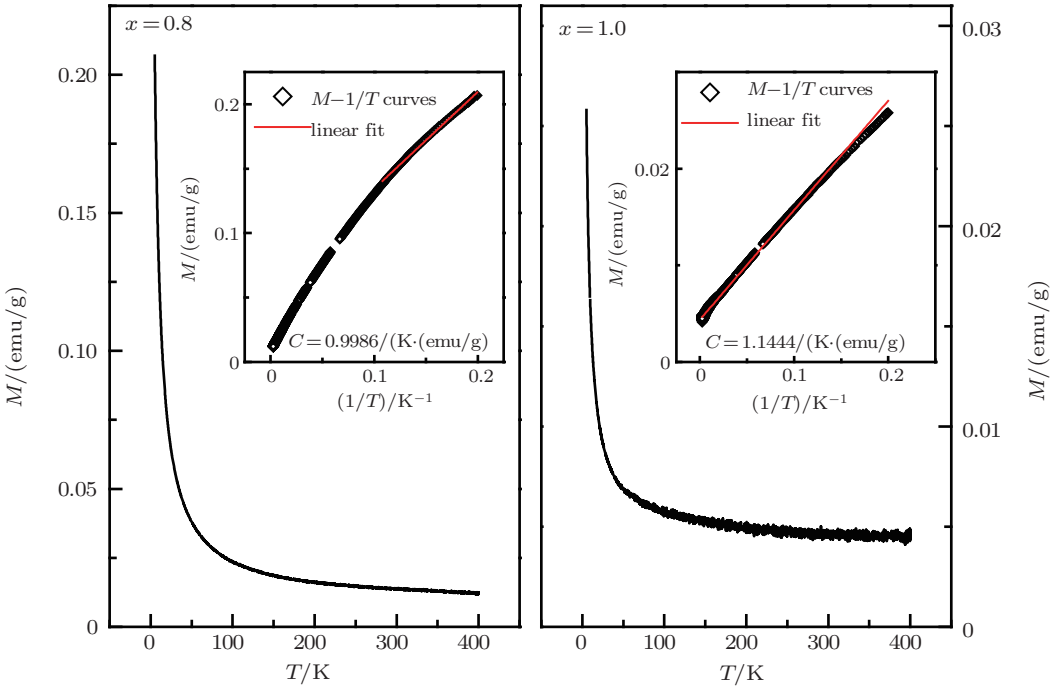


Fig. 7. (color online) Temperature-dependent magnetization curves of $SmFe_{(1-x)}Al_xO_3$ ($x = 0.8$, 1.0) under an applied field $H =$ 1 kOe, with the inset showing the linear fit of $M - 1/T$ curves.

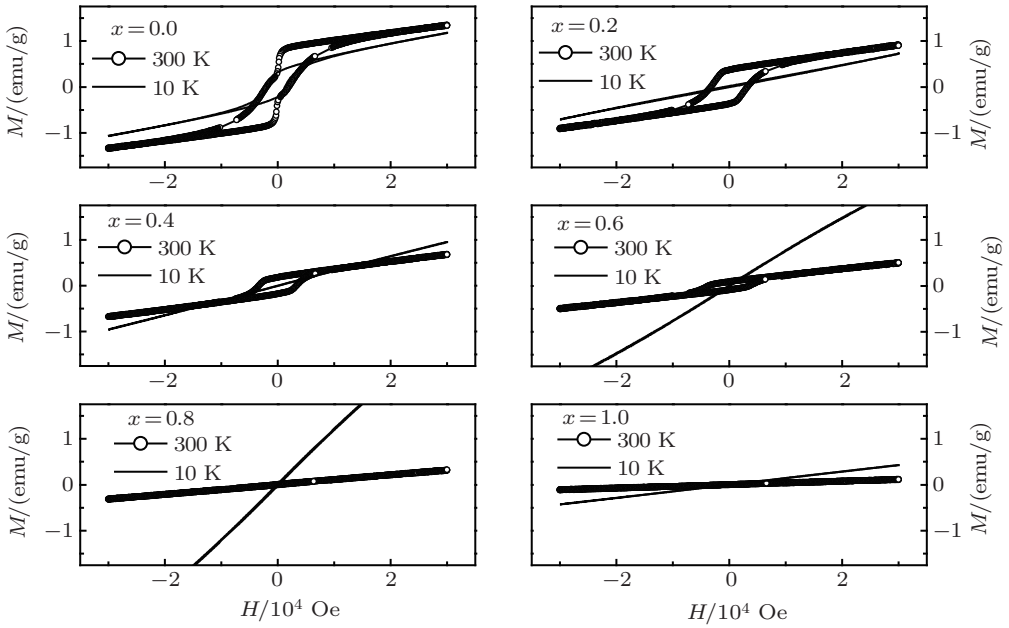


Fig. 8. Magnetic field-dependent magnetizations of $SmFe_{(1-x)}Al_xO_3$ ($x = 0.0$, 0.2, 0.4, 0.6, 0.8, 1.0) measured up to 30 kOe at $T = 10$ K, 300 K, respectively.

In order to gain an insight into the alignment of the magnetic domains which contributes to the effective magnetic characteristics of $SmFe_{(1-x)}Al_xO_3$ ($0 \leq x \leq 1$), the isothermal magnetization hysteresis loops are measured at 10 K and 300 K, respectively. As shown in Fig. 8, we can clearly see the different magnetic behaviors of $SmFe_{(1-x)}Al_xO_3$. At room temperature, a typical ferromagnetic hysteresis loop occurs for $0 \leq x \leq 0.6$, while the saturated magnetization and coercivity decrease gradually with Al concentration increasing. The samples of $x = 0.8$ and 1.0 take on paramagnetic behaviors. At 10 K, the ferromagnetic hysteresis loops are only observed for $x = 0$ and 0.2, and the others show paramagnetic characteristics. The dramatic changes in the magnetization hysteresis loops indicate that the paramagnetic behavior of Sm^{3+} sublattices dominates over the system at lower temperature. Here all the results have subtracted the diamagnetic background signals.

4. Conclusion

In conclusion, the structural and magnetic properties of $SmFe_{(1-x)}Al_xO_3$ ($0 \leq x \leq 1$) have been investigated in detail. It is found that the octahedral tilting distortions of FeO_6 are alleviated with the increase of doped Al content. In the whole composition range, each of all the samples remains an orthorhombic structure with space group *Pbnm*. The lattice constants a_{pc}, b_{pc}, and c_{pc} decrease with the increase of Al concentration. However, deviation from Vegard's rule is observed and it can be caused by the magnetostriction effect since the magnetic behavior changes from ferromagnetic to paramagnetic one with the increase of Al doping content. Subsequently the magnetic properties of $SmFe_{(1-x)}Al_xO_3$ ($0 \leq x \leq 1$) are studied. From the M–T curves of $SmFe_{(1-x)}Al_xO_3$, the doping of nonmagnetic Al can break the symmetry of the local interactions, leading to the decompensation of Fe^{3+}–Fe^{3+} antiferromagnetic interactions in their environment and weakening the interaction between the Fe^{3+}–Sm^{3+}. As a result, the magnetization and the spin reorientation temperature (T_k) monotonically decrease as the Al content increases for $0 \leq x \leq 0.6$. The iron atoms decrease drastically, which makes the magnetic interaction between Fe^{3+} and Sm^{3+} ions very weak for $0.8 \leq x \leq 1$. And the magnetic properties are mainly determined by magnetic interactions of Sm^{3+}–Sm^{3+}, and they exhibit paramagnetic behavior. The isothermal magnetization hysteresis loops measured at 10 K and 300 K for $SmFe_{(1-x)}Al_xO_3$ ($0 \leq x \leq 1$) indicate that the magnetic interaction is weakened with the increase of doping Al content, and the paramagnetic behavior of Sm^{3+} sublattices dominates over the system at lower temperature.

References

[1] Wu A, Cheng G, Shen H and Xu J 2009 *J. Chem. Eng.* **4** 518
[2] Shen S T and Weng H S 1998 *Ind. Eng. Chem. Res.* **37** 2654
[3] Kharton V V, Yaremchenko A A, Kovalevsky A V, Kovalevsky A P, Naumovich E N and Kerko P F 1999 *J. Membr. Sci.* **163** 307
[4] Kharton V V, Yaremchenko A A and Naumovich E N 1999 *J. Solid State Electrochem.* **3** 302
[5] Kuscer D, Hrovat M, Hoic J, Bernik S and Kolar D 1996 *J. Power Sources* **61** 161
[6] Traversa E, Matsushima S, Okada G, Sadaoka Y, Sakai Y and Watanabe K 1995 *Sens. Actuators B* **25** 661
[7] Schmool D S, Keller N, Guyot M, Krishnan R and Tessier M 1999 *J. Appl. Phys.* **86** 5712
[8] Sakakima H, Satomi M, Hirota E and Adachi H 1999 *IEEE Trans. Magn.* **35** 2958
[9] Zheng L and Wu X S 2013 *Chin. Phys. B* **22** 107806
[10] Yang Y, Liu Y L, Zhu K, Zhang L Y, Ma S Y, Liu J and Jiang Y J 2010 *Chin. Phys. B* **19** 037802
[11] Wang H C, Wang C L, Zhang J L, Zhao M L, Liu J, Su W B, Yin N and Mei L M 2009 *Chin. Phys. Lett.* **26** 107301
[12] Prasad B V, Rao G N, Chen J W and Babu D S 2011 *Mater. Res. Bull.* **46** 1670
[13] Kahn F J, Pershan P S and Remeika J P 1969 *Phys. Rev.* **186** 891
[14] Lee J H, Jeong Y K, Park J H, Oak M A, Jang H M, Son J Y and Scott J M 2011 *Phys. Rev. Lett.* **107** 117201
[15] Kadomtseva A M, Zvezdin A K, Lukina M M, Milov V N, Mukhin A A and Ovchinnikova T L 1977 *Zh. Eksp. Teor. Fiz.* **46** 1216
[16] Derkachenko V N, Zvezdin A K, Kadomtseva A M, Kovtun N M, Lukina M M and Mukhin A A 1984 *Phys. Status Solidi A* **84** 215.
[17] Bartolome F and Bartolome J 2005 *Solid State Sci.* **7** 700
[18] Zvezdin A K, Kadomtseva A M and Mukhin A A 1980 *IZV. Akad. Nauk SSSR Ser. Fiz.* **44** 1348
[19] Larson A C and Von Dreele R B 2004 *General Structure Analysis System (GSAS) Los Alamos National Laboratory Report LAUR* **86** 748
[20] Lufaso M W and Woodward P M 2001 *Acta Crystallogr., Sect. B: Struct. Sci.* **57** 725
[21] Bombik A, Leśniews B, Mayer Jacek, Oleś A, Pacyna A W and Przewoźnik J 1997 *J. Magn. Magn. Mater.* **168** 139
[22] Maslen E N, Stretsov V A and Ishizawa N 1996 *Acta Crystallogr., Sect. B: Struct. Sci.* **52** 406
[23] Lacorre P, Torrance J B, Pannetier J, Nazzal A I, Wang P W and Huang T C 1991 *J. Solid State Chem.* **91** 225
[24] Bashira A, Ikrama M, Kumarb R, Lisboa-Filho P N and Thakur P 2010 *Mater. Sci. Eng. B* **172** 242